CHEMISTRY
A European Journal

A Journal of
ChemPubSoc Europe

Accepted Article

Title: Mesoporous silica scaffolds as precursors to drive the formation of hierarchical SAPO-34 with tunable acid properties

Authors: Ivana Miletto, Geo Paul, Sthepanie Chapman, Giorgio Gatti, Leonardo Marchese, Robert Raja, and Enrica Gianotti

To be cited as: *Chem. Eur. J.* 10.1002/chem.201701978

Link to VoR: http://dx.doi.org/10.1002/chem.201701978

Supported by
ACES

WILEY-VCH

10.1002/chem.201701978

WILEY-VCH

Mesoporous silica scaffolds as precursor to drive the formation of hierarchical SAPO-34 with tunable acid properties

I. Miletto,[a] G. Paul,[a] S. Chapman,[b] G. Gatti,[a] L. Marchese,[a] R. Raja[b] and E. Gianotti*[a]

Abstract: Using a distinctive bottom-up approach, hierarchical SAPO-34 has been synthesized using CTAB encapsulated within ordered mesoporous silica (MCM-41) that serves as both the silicon source and mesoporogen. The structural and textural properties of the hierarchical SAPO-34 were contrasted against its microporous analogue, and the nature, strength and accessibility of the Brønsted acid sites were studied using a range of physicochemical characterization tools; notably probe-based FTIR and solid-state (SS) MAS NMR. Whilst CO was used to study the acid properties of hierarchical SAPO-34, bulkier molecular probes (including pyridine, 2,4,6-trimethylpyridine and 2,6-di-*tert*-butylpyridine) allowed particular insight into the enhanced accessibility of the acid sites. The activity of the hierarchical SAPO-34 catalyst was evaluated in the industrially-relevant, acid-catalysed Beckmann rearrangement of cyclohexanone oxime to ε-caprolactam, under vapor-phase conditions. These catalytic investigations revealed a significant enhancement in the yield of ε-caprolactam using our hierarchical SAPO-34 catalyst compared to SAPO-34, MCM-41, or a mechanical mixture of these two phases. The results highlight the merits of our design strategy for facilitating enhanced mass transfer, whilst retaining favorable acid site characteristics.

Introduction

The application of microporous zeolitic materials as industrial solid-acid catalysts has been extensive, reflecting the potent combination of their molecular sieving capabilities and scope of their catalytic properties [1,2]. Among zeolite-type materials, the silicoaluminophosphates (SAPOs) represent a viable alternative to aluminosilicates for applications requiring acid catalysis [3,4]. In particular, SAPO-34 (CHA topological structure) has been investigated extensively due to its potential application in CO_2/CH_4 separation [5] and hydrogen purification [6], in addition to its well-established industrial role in the methanol-to-olefin (MTO) process (100% methanol conversion and >90% selectivity to C_2-C_4 light olefins) [7-9]. Nevertheless, the small, 8-ring pore aperture (3.8x3.8 Å) and large CHA cavity (9.4 Å in diameter) impose diffusion limitations and expedite catalyst deactivation through coke formation/deposition [10].

To overcome these drawbacks, hierarchical SAPO-34, which combines the microporous CHA structure with an additional mesoporous network, has been prepared using both top-down [11-13] and bottom-up [14,15] approaches. Generally, top-down approaches involve post-synthetic modification, such as demetallation under acidic or basic conditions, to extract framework constituents whilst preserving crystallinity. Localized collapse of the zeolite framework generates mesoporous voids but simultaneously elicits defect sites, thus irrevocably altering both the textural and acid characteristics of the parent framework [16]. Although demetallation has been widely employed for the production of hierarchical zeolites [17,18], comparably few examples have been reported for silicoaluminophosphates [11,12] due to the their relative instability under strongly acidic or alkaline conditions [11]. Often, a bottom-up approach is employed for the production of hierarchical SAPOs, whereby sophisticated, but sacrificial, surfactant molecules self-assemble into a supramolecular micelle that guides the formation of the mesoporous network, whilst a structure-directing agent facilitates the formation of the microporous architecture. The bottom-up approach is relatively facile, being compatible with a 'one-pot' synthesis, and benefits from a high degree of structural control through the modification of the micellar structure (by the choice of surfactant molecule and the use of additives, such as swelling agents) [16]. Typically the surfactants used to synthesize hierarchical SAPOs in the bottom-up approach are organosilanes such as TPOAC ([3-(trimethoxysilyl)propyl]-octa-decyldimethyl ammonium chloride) [19]. These molecules incorporate a trimethoxysilyl moiety that can form covalent bonds with zeolitic precursors, promoting the crystallization of a single, hierarchical phase [20]. Nonetheless, the bottom-up approach can have a detrimental impact on material crystallinity and, moreover, the use of amphiphilic organosilane templates leads to the incorporation of siliceous species into the walls of the mesopores, modifying the acid characteristics of the parent framework [15].

Herein we report a novel, facile, bottom-up approach for the preparation of hierarchical SAPO-34 (designated HierSAPO-34) acid catalyst, mitigating the need for sophisticated surfactants, instead using CTAB encapsulated within ordered mesoporous silica (MCM-41) that serves as both the silicon source and mesoporogen. This method benefits from superior retention of the desirable acid properties of the microporous parent framework, whilst simultaneously enhancing its mass transport capabilities. The HierSAPO-34 catalyst was fully characterized using FTIR spectroscopy of adsorbed probe molecules, together with solid-state (SS) MAS-NMR. In addition, the structural and textural properties of the HierSAPO-34 were evaluated using X-ray diffraction (XRD) and volumetric analyses. FTIR

[a] Dr I. Miletto, Dr G. Paul, Dr G. Gatti, Prof. L. Marchese and Prof. E. Gianotti
Department of Science and Technological Innovation, Università del Piemonte Orientale, Viale T. Michel 11, 15121 Alessandria, Italy.
E-mail: enrica.gianotti@uniupo.it
[b] Mrs S. Chapman and Prof. R. Raja
School of Chemistry, Faculty of Natural and Environmental Sciences, University of Southampton, SO17 1BJ, U.K.

Supporting information for this article is given via a link at the end of the document.

spectroscopy of adsorbed probe molecules of varying kinetic diameters is a powerful tool in the systematic study of the acid properties of hierarchical zeolites, providing information on the location, content, strength and accessibility of both Brønsted and Lewis sites [18,21,22]. In this study, CO was used to assess the acid strength of the HierSAPO-34, whilst strongly-basic molecules of increasing kinetic diameter, including ammonia, pyridine, 2,4,6-trimethylpyridine (collidine) and 2,6-di-*tert*-butylpyridine, were used to probe the accessibility of these sites. As a probe molecule, NH_3 is sufficiently small and basic to be adsorbed and protonated by all the Brønsted acid sites in both the micro- and meso-pores of the HierSAPO-34. Larger probe molecules, such as alkylpyridines, with kinetic diameters exceeding the micropore dimensions, can only assess those Brønsted acid sites present in the mesopores or at the mouth of the micropores. Such probe-based studies are particularly pertinent to catalysis for their role in establishing structure-property relationships. These analyses can facilitate mechanistic studies that ultimately aid further catalyst optimization. To this end, the acid characteristics of HierSAPO-34 have been studied in the vapor-phase, acid-catalyzed Beckmann rearrangement of cyclohexanone oxime; a fundamental step in the production of ε-caprolactam (the monomeric precursor to the Nylon-6 polymer). These perspicacious spectroscopic studies highlight how framework topology and acid-site characteristics influence catalyst activity in the context of an industrially-relevant catalytic process.

Results and Discussion

Hierarchical SAPO-34 (HierSAPO-34) was synthesized using a soft-templating strategy in which pre-synthesized MCM-41, with the surfactant (CTAB) inside the mesopores, was used as both the silicon and surfactant source (Scheme 1). The addition of CTAB-containing MCM-41 to the reaction mixture instigates the gradual dissolution of the silica framework (Step 1, Scheme 1) with subsequent formation of silicic acid monomers that provide a silicon source for the formation of the SAPO-34 framework (Step 2, Scheme 1). For comparison, a microporous SAPO-34 was synthesized under identical synthesis conditions, employing TEOS as the silicon source. In HierSAPO-34, the presence of the CTAB in the mesopores might slacken the hydrolysis rate and collapse of the silica framework; as a consequence, SAPO-34 crystallization might preferentially take place along the CTAB-templated MCM-41 pore system [24]. SEM imaging reveals that the morphology of HierSAPO-34 (Fig.1A) differs from both its microporous analogue (Fig. S1A) and also mesoporous MCM-41 (Fig. S1B). Significantly, energy-dispersive X-ray (EDX) spectroscopic analyses (Fig. 1B) collected in different areas of the HierSAPO-34 sample reveals a homogeneous distribution of Al, P and Si, with no evidence of MCM-41-type particles. In addition, the Si/(Si+Al+P) ratio for HierSAPO-34, determined by inductively-coupled plasma (ICP) analysis (Table 1), is in good agreement with the synthesis gel composition. Thus, our textural and compositional analysis of HierSAPO-34 provides strong evidence in support of a homogeneous hierarchical phase.

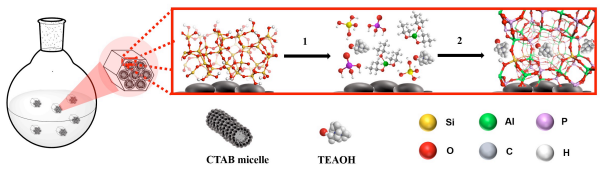

Scheme 1. Depiction of the synthesis of HierSAPO-34 using CTAB encapsulated within MCM-41 as both the silicon source and mesoporogen.

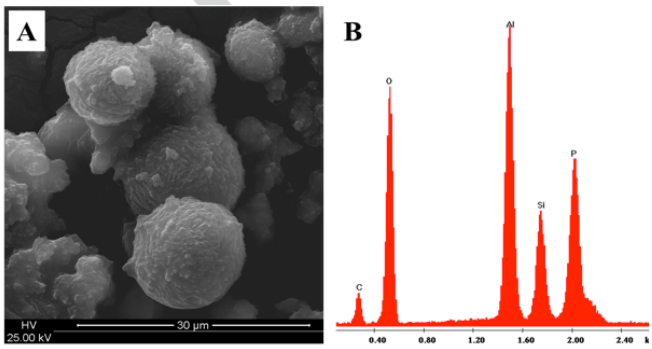

Figure 1. Representative SEM image (A) and energy-dispersive X-ray spectroscopic microanalysis (B) of HierSAPO-34.

The XRD pattern of HierSAPO-34 reveals the characteristic diffraction peaks of the CHA structure (Fig. 2A), thus confirming the phase purity and crystallinity of the sample. In addition, in the low-angle range (Fig. 2A, inset), HierSAPO-34 exhibits a diffraction peak at *ca.* 2° that is indicative of ordered mesoporosity. The low-angle peak is notably absent for microporous SAPO-34. The presence of both micro- and meso-porosity in HierSAPO-34 was also evidenced by N_2 adsorption/desorption analysis at 77 K (Fig. 2B and 2C).

Table 1. Inductively-coupled plasma (ICP) chemical analysis of SAPO-34 Catalysts.

Catalyst	Si wt. %	Al wt. %	P wt. %	[a]Si/ Si+Al+P	[b]Si/ Si+Al+P
HierSAPO-34	11.44	18.72	10.71	0.28	0.23
SAPO-34	3.19	17.56	15.92	0.08	0.07

[a] Experimental framework composition determined by ICP analysis after the synthesis. [b] Theoretical framework composition determined from the synthesis gel composition.

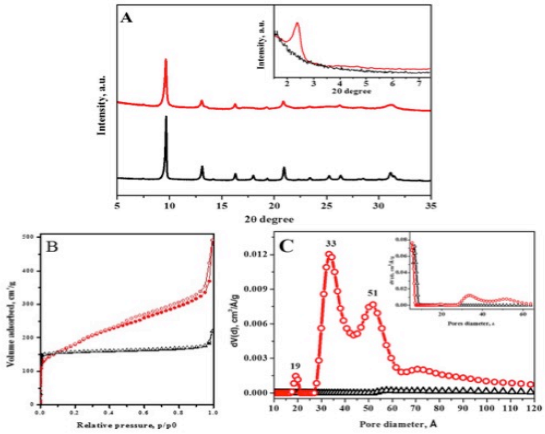

Figure 2. A: The powder XRD pattern of microporous SAPO-34 (black) and HierSAPO-34 (red), with the low-angle region (inset A). B: The N_2 adsorption/desorption isotherms at 77K. C: The pore size distribution in the mesopore range, with pore size distribution in the micropore and mesopore range (inset C).

Whilst the isotherm of microporous SAPO-34 is archetypical Type I, enhanced N_2 uptake at intermediate and high pressures by HierSAPO-34 yields a Type IV isotherm, which is characteristic of mesoporous materials. Pore size distributions (Fig. 2C) for SAPO-34 and HierSAPO-34 were determined by invoking NLDFT (non-localized density functional theory) to analyze the desorption branch of their respective isotherms [25-27]. Encouragingly, the pore size distribution of SAPO-34 was consistent with the microporous CHA structure (Fig. 2C, inset), whilst HierSAPO-34 exhibits additional microporosity at 19 Å, as well as mesopores of 33 and *ca.* 70 Å diameter (Fig. 2C).

Details of the specific surface area and pore volumes, determined by the NLDFT method, are summarized in Table 2. Significantly, with respect to microporous SAPO-34, the HierSAPO-34 exhibits substantial enhancements in mesopore volume (V_{meso}) and total pore volume (V_{tot}), with concomitant reduction in micropore volume (V_{micro}), and mesopore surface area (S_{meso}) is greatly enhanced in the hierarchical material. Volumetric data strongly supports the successful preparation of hierarchical architectures, and indicates the coexistence of multiple levels of porosity within HierSAPO-34.

To probe the chemical environment of the framework atoms in both microporous and HierSAPO-34, ^{27}Al, ^{31}P and ^{29}Si MAS NMR characterization was performed (Fig. 3). The ^{27}Al spectra of both SAPO-34 and HierSAPO-34 exhibit a single signal at *ca.* 36 ppm, which can be attributed to the tetrahedrally-coordinated Al atoms of $Al(OP)_4$ (Fig. 3A). The absence of a signal at -13 ppm precludes octahedrally-coordinated, extra-framework Al sites. In both microporous and hierarchical samples, a peak at approximately -29.8 ppm in the ^{31}P NMR spectra is assigned to tetrahedrally-coordinated P atoms (Fig. 3B). Since both ^{27}Al and ^{31}P NMR spectra exhibit only a single resonance, it is possible to confirm strict alternation of Al and P at the T-positions of the aluminophosphate framework [28].

In the ^{31}P NMR spectrum of HierSAPO-34, a broad foot beneath the main peak (centered at approximately -24 ppm) might be attributed to P-OH, or otherwise indicate changes in the second coordination sphere due to Al speciation. It is likely that such changes are not reflected in the corresponding ^{27}Al NMR spectra due to broadening beyond detection [29]. The ^{29}Si cross-polarization (CP) MAS NMR spectra of microporous SAPO-34 revealed multiple signals at -92, -96 and -101 ppm due to tetrahedrally-coordinated framework silicon coordinated to four, three, and two Al atoms, respectively (Fig. 3C). These three characteristic signals are also present in HierSAPO-34, though broadened by the presence of silicon islands $Si(OSi)_4$) or aluminosilicate islands $Si[(OSi)_l(OAl)_m(OH)_n]$ in the SAPO framework [1,12,30,31]. The ^{29}Si CP MAS NMR spectrum of calcined MCM-41 is included in the supplementary information (Fig. S2).

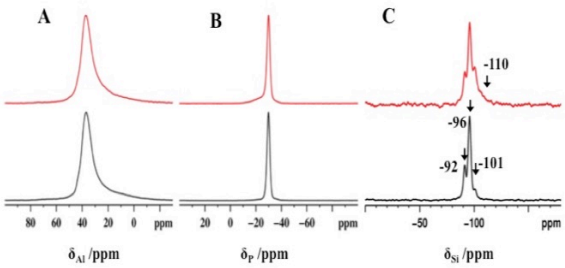

Figure 3. The ^{27}Al (A), ^{31}P (B) MAS NMR, and ^{29}Si (C) CP MAS NMR spectra of calcined hierarchical SAPO-34 (red) and SAPO-34 (black)

Table 2. Textural properties of the SAPO-34 and HierSAPO-34.

Catalysts	S_{BET} $m^2 g^{-1}$	S_{DFT} $m^2 g^{-1}$	S_{micro} $m^2 g^{-1}$	[a] S_{meso} $m^2 g^{-}$	[b] Relative mesopore area [%]	$V_{tot\ DFT}$ $cm^3 g^{-1}$	V_{micro} $cm^3 g^{-1}$	V_{meso} $cm^3 g^{-1}$	[c] Relative mesopore volume[%]
SAPO-34	477	819	811	8	0.98	0.26	0.23	0.03	12.9
HierSAPO-34	641	783	511	272	34.7	0.58	0.13	0.44	76.7
MCM-41	1110	1267	-	-	-	1.3	-	1.3	-

[a] $S_{meso} = S_{DFT} - S_{micro}$; [b] Relative mesopore area = S_{meso}/S_{DFT} x 100 ; [c] Relative mesopore volume= $V_{meso}/V_{tot.DFT}$ x 100.

^{1}H MAS NMR, coupled with FTIR spectroscopy of adsorbed molecules, was used to establish the nature and strength of the acid sites present in microporous and hierarchical SAPO-34. In the OH stretching region of FTIR spectra (Fig. 4A), microporous SAPO-34 displays two intense bands with maxima at 3630 and 3600 cm^{-1}. These bands are assigned to the O-H stretching mode of Al(OH)Si Brønsted acid sites (BAS) of different acid strengths, in the O4 (3630 cm^{-1}) and O2 (3600 cm^{-1}) structural configurations of the CHA framework [30-33]. Hierarchical SAPO-34 shows the same bands due to the Brønsted acid sites, though at lower intensity, as well as additional signals arising from isolated Si-OH (3745 cm^{-1}) and isolated P-OH (3678 cm^{-1}) sites. In addition, a very broad signal from 3550-3350 cm^{-1} is visible due to the presence of hydrogen-bonded hydroxyls [18]. Importantly, the detection of the characteristic BASs of SAPO-34 within the HierSAPO-34 material confirms the dissolution of MCM-41 network and the successful incorporation of the Si into the CHA architecture.

In conjunction with FTIR studies, ^{1}H MAS NMR spectroscopy has provided direct information about the different proton sites present in these samples (Fig. 4B) and quantitative representations of the various protonic species are shown in Table 3. A signal at around 4 ppm, associated with Brønsted Si(OH)Al groups, is present in both microporous and hierarchical SAPO-34. After deconvolution, two components at 3.6 ppm and 3.9 ppm can be identified, corresponding to the two types of Brønsted acid sites in the CHA framework. The quantity of BAS groups calculated using ^{1}H MAS NMR is lower in HierSAPO-34 than in its microporous analogue. Aside from the BASs, a signal at lower chemical shift can be identified in the spectrum of HierSAPO-34 only. This resonance is of composite nature and subsequent deconvolution revealed two signals at 2.0 and 1.8 ppm. Whilst the signal at 1.8 ppm is due to external silanols (Si-OH$_{ext}$) at lattice defects, the signal at 2.0 ppm can be attributed to Si-OH groups interacting with neighboring oxygen atoms (Si-OH$_{int}$), identifying their intra-framework location [34-37].

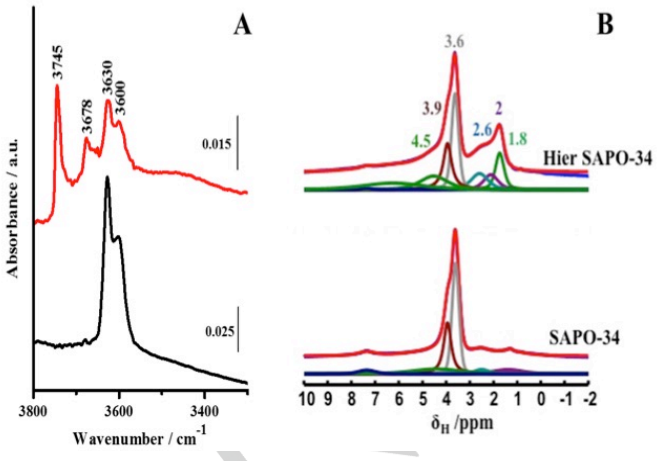

Figure 4. FTIR spectra in the O-H stretching region (A) and ^{1}H MAS NMR spectra (B) of calcined microporous SAPO-34 (black) and hierarchical SAPO-34 (red).

Table 3. FTIR frequencies and population distribution of protonic species obtained from single-pulse ^{1}H MAS NMR spectroscopy in microporous and hierarchical SAPO-34.

ν_{OH} /cm^{-1}	^{1}H chemical shift (δ) /ppm	Assignment	^{1}H species HierSAPO-34	% SAPO-34
3745	1.8	Si-OH$_{ext}$	12	-
3745 tail	2.0	Si-OH$_{int}$	8	-
3678	2.6	P-OH	10	4
3630	3.6	BAS	23	42
3600	3.9	BAS	17	27
3550-3350	≈ 4.5	H-bonded species	30	18

These two distinct groups of silanols are indistinguishable by FTIR due to the overwhelming signal of external Si-OH, although a pronounced tail on the band at 3745 cm^{-1} does suggest the presence of another type of silanol site. A weak signal at 2.6 ppm, due to P-OH species, is also present in HierSAPO-34. Proton resonances beyond 4.5 ppm are attributed to hydrogen-bonded species, and are related to the broad 3550-3350 cm^{-1} signal in the corresponding FTIR spectrum [18]. In contrast, the ^{1}H NMR spectrum of calcined MCM-41 shows only a sharp peak at 1.8 ppm due to Si-OH groups, and a broad feature in the range of 2-6 ppm (Fig. S3).

To assess the accessibility and strength of acid sites in HierSAPO-34, probe molecules of varying basicity and steric hindrance were adsorbed and their interactions studied by FTIR spectroscopy. Initially, CO was used as a probe molecule since, due to its weak basicity; it is particularly effective at discriminating acid sites of different strength. In particular, the adsorption of CO at 80 K leads to the formation of OH···CO hydrogen-bonded adducts with acid sites, and the degree of the concomitant shift of the hydroxyl band ($\Delta\nu_{OH}$) can be correlated with catalyst acidity [38-41]. In Figure 5, the FTIR spectra of CO adsorbed at 80 K on HierSAPO-34 (A) and SAPO-34 (B) are shown. For both catalysts, adsorption of CO at low temperature causes the bands of the Si(OH)Al Brønsted acid sites (3630 and 3610 cm^{-1}) to downshift due to the formation of OH···CO H-bonded adducts, yielding a broad, intense absorption centered at *ca.* 3350 cm^{-1}. As the degree of redshift is similar for both microporous and hierarchical SAPO-34, their Brønsted acid sites are of similar strength. At low CO coverage, the C-O stretching region reveals a signal centered at 2170 cm^{-1} corresponding to the stretching mode of CO interacting with Brønsted acid sites. Whilst this CO stretching mode is present in the spectra of both catalysts, its intensity varies between the microporous and hierarchical SAPO-34. The observed blue-shift (32 cm^{-1}) with respect to the stretching mode of the free CO molecule (ν_{CO} liquid-like at 2138 cm^{-1}) is similar for both samples, again highlighting their comparable acid strength. However, on progressing to a high pressure of CO, the band at 2170 cm^{-1} for HierSAPO-34 presents a low-frequency tail, which can be ascribed to the stretching mode of CO interacting with Si-OH and P-OH groups. At high CO coverage, HierSAPO-34 (Fig. 5A) exhibits a shoulder at 3470 cm^{-1} due to CO interaction with the P−OH defects [42], but signals arising from the interaction of CO with Si-OH groups is imperceptible due to overlap with the

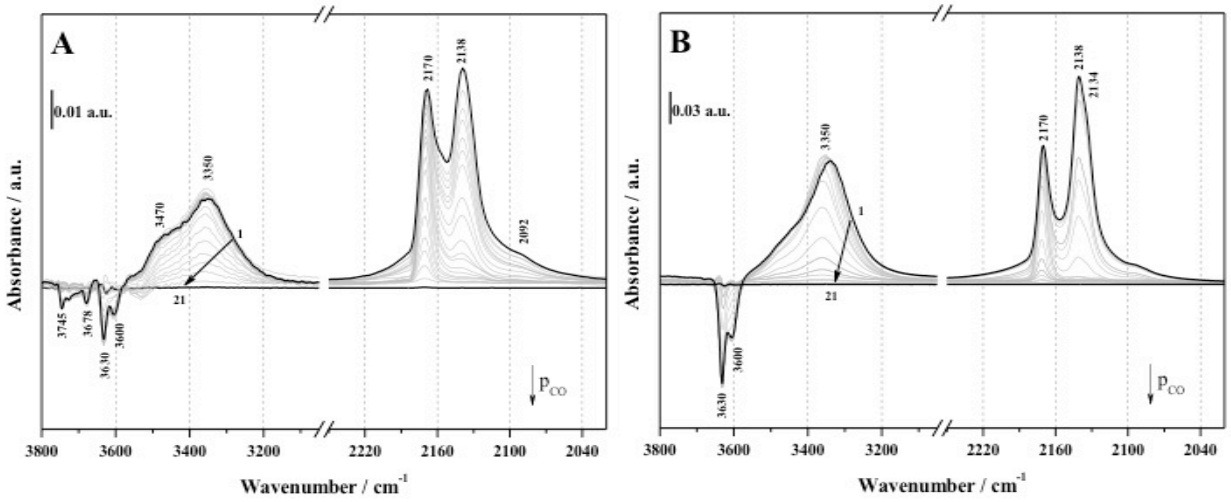

Figure 5. FTIR difference spectra in the O-H (high frequency, 3800 – 3100 cm^{-1}) and C-O (low frequency, 2220 – 2040 cm^{-1}) stretching region of CO adsorbed at 80 K on HierSAPO-34 (A) and SAPO-34 (B) catalysts. Curve 1: Adsorption of 15 mbar of CO, Curves 1 to 21: decreasing CO doses up to 1 x10^{-4} mbar.

negative bands in the 3650-3590 cm^{-1} range. The adsorption of CO at low temperature shows that the Brønsted acid sites of the hierarchical catalyst are of similar strength to those in microporous SAPO-34, indicating that the overall acid characteristics of SAPO-34 are retained in the hierarchical system. However, due to its small diameter, CO is unable to discriminate acid sites based on their location within the hierarchical framework. In order to discriminate the Brønsted acid sites located inside the micropores from those present on the mesopore surface, probe molecules of significantly larger kinetic diameter were employed. Substituted pyridines are appropriate probe molecules as their inherent basicity and steric bulk (which restricts diffusion through small pore apertures) can be exploited in qualitative and quantitative analysis of acid site accessibility [4,18,43-47]. In particular, pyridine (Py) with a kinetic diameter of 0.54 nm, 2,4,6-trimethylpyridine (2,4,6-TMP, collidine) with a kinetic diameter approximately 0.74 nm, and 2,6-di-tert-butyl-pyridine (2,6-dTBP) with a kinetic diameter of 1.05 nm, are too large to enter the micropores of SAPO-34 and thus can only interact with acid sites located within the mesopores or at the micropore mouths. These interactions are readily identified using FTIR, both through the characteristic aromatic ring vibrations of the probe molecule and, owing to their basicity, through their conjugate acid (PyH$^+$, 2,4,6- TMPH$^+$ and 2,6-dTBPH$^+$) formed by proton transfer at a Brønsted acid site.

Fig. 6 reports the FTIR spectra of adsorbed 2,4,6-TMP at room temperature on HierSAPO-34. In the O-H stretching region (Fig. 6A), the 3630 and 3600 cm^{-1} bands of the Brønsted acid sites are only partially eroded upon contact (10 min) with 2,4,6-TMP vapor pressure (red curve). Concurrently, at lower frequencies, new bands at 3295 cm^{-1}, due to the N-H$^+$ stretching mode of protonated 2,6-dTBP, at 3040 cm^{-1}, due the C-H stretching mode of pyridine ring and at 2975 and 2930 cm^{-1} due to symmetric and asymmetric stretching mode of methyl groups, are formed [48]. Overall, this behavior suggests that only a fraction of the Brønsted acid sites are accessible to the 2,4,6-TMP molecules. In the aromatic C-C ring vibration range (Fig. 6B), the ν_{8a} mode, which in the liquid phase appears at 1611 cm^{-1}, is very sensitive to the presence of the BASs of the catalysts, its position changing with acid strength. When the ν_{8a} mode appears at wavenumbers in excess of 1630 cm^{-1}, it can be associated with the formation of the protonated species (2,4,6-TMPH$^+$), whereas a lower wavenumber indicates the formation of a hydrogen-bonded adduct [4,18,45,49]. Upon interaction with 2,4,6-TMP, bands at 1618 and 1574 cm^{-1} due to hydrogen bonding to Si-OH groups, and a band 1638 (ν_{8a}) cm^{-1} with a shoulder at 1650 (ν_{8b}) cm^{-1} due to 2,4,6-TMPH$^+$, are observed. The latter was found to be relatively resistant to thermal treatment, testifying the interaction of 2,4,6-TMP with strong Brønsted acid sites in HierSAPO-34. In fact, after outgassing the catalyst at 373K, the band at 1638 cm^{-1} due to the protonated species 2,4,6-TMPH$^+$ is retained, whilst those of the hydrogen-bonded adduct (1618 and 1574 cm^{-1}) are lost (Fig. S4). The 1638 cm^{-1} band is not present in the FTIR spectrum of microporous SAPO-34 (Fig. 6C, black curve), where only a signal at 1611 cm^{-1}, due to physisorbed 2,4,6-TMP, is visible. The presence of the 1638 cm^{-1} band in the spectrum of HierSAPO-34 evidences the enhanced accessibility of the Brønsted acid sites, facilitated by its mesoporous network. To gain further insight into the fraction of accessible Brønsted sites in HierSAPO-34, other strongly-basic probe molecules, of different kinetic diameter were deployed. In particular, NH_3 was used to monitor the total Brønsted acid sites, as it readily enters both the micropores and mesopores of the HierSAPO-34 framework [50,51], whereas pyridine (Py), with a kinetic diameter of 0.54 nm, and 2,6-di-tert-butylpyridine (2,6-dTBP), with a kinetic diameter of 1.05 nm, cannot enter the micropores and can therefore probe only the more accessible acid sites [47]. The FTIR difference spectra of NH_3 (Fig. 7A), pyridine (Fig. 7B) and 2,6-dTBP (Fig. 7C) adsorbed on HierSAPO-34 at room temperature are reported in the low frequency region where the signals of protonated species are observed.

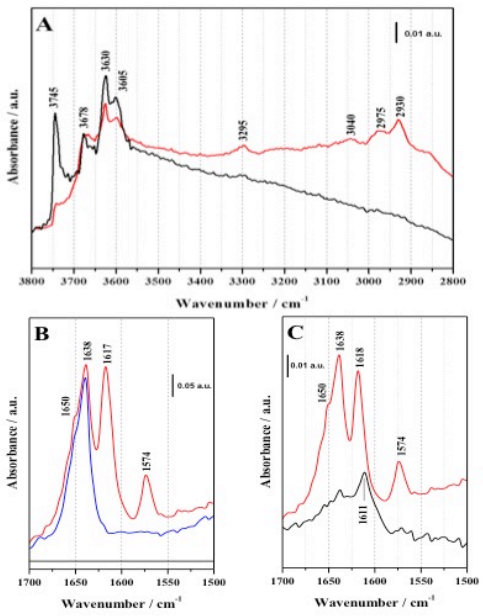

Figure 6. FTIR absorbance spectra in the O-H stretching region (A) and FTIR difference spectra in the aromatic ring vibration range (B) of 2,4,6-TMP adsorbed on HierSAPO-34. The black curve is the spectrum of HierSAPO-34 in vacuum, red curve upon 10 minutes of contact time with 2,4,6-TMP vapor pressure and the blue curve is related to the 2,4,6-TMP desorption at 373K. A comparison of the FTIR difference spectra of HierSAPO-34 (red curve) and of SAPO-34 (black curve) upon contact with 2,4,6-TMP vapor pressure is also provided (C).

Upon adsorption of 100 mbar of NH_3 (Fig. 7A, red curve), the bending mode of ammonia hydrogen-bonded to silanols is detected by a band at 1620 cm^{-1}. Furthermore, the asymmetric bending mode of the NH_4^+ ions (1450 cm^{-1}), reveals that proton transfer has occurred between the Brønsted acid sites of HierSAPO-34 and ammonia. In the ring-stretching region, adsorption of pyridine on HierSAPO-34 (Fig. 7B, red curve) produces bands due to physisorbed pyridine (1580 ν_{8b}, 1481 ν_{19a} and 1438 ν_{19b} cm^{-1}), pyridine hydrogen-bonded to silanols (1596 ν_{8b} and 1445 ν_{19b} cm^{-1}), and protonated species from interaction with strong Brønsted acid sites (1634 ν_{8a}, 1623 ν_{8b}, 1545 ν_{19b} and 1488 ν_{19a} cm^{-1}) [52]. Upon outgassing the sample at room temperature (Fig. 7B, black curve), the bands due to physisorbed pyridine are removed. Finally, adsorption of 2,6-di-tert-butylpyridine (Fig. 7C) produces a band at 1618 cm^{-1} due to protonated 2,6-dTBPH$^+$ species, and a band at 1600 cm^{-1}, due to hydrogen bonding interactions with Si-OH groups.[47] Subsequent outgassing of the sample at 298K (Fig. 7C, black curve) removes the band associated with interaction between Si-OH and 2,6-dTBPH, whilst the intensity of the band due to the protonated species is gradually reduced on outgassing the sample at higher temperatures (Fig. S5-S7).

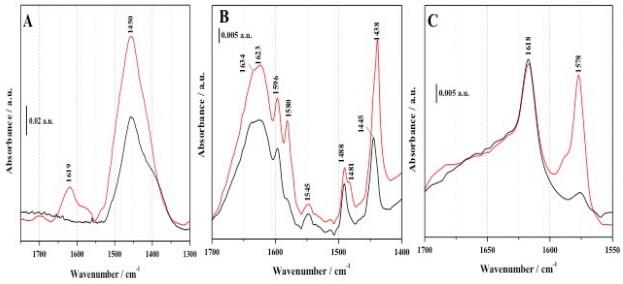

Figure 7. FTIR difference spectra of HierSAPO-34 on adsorption of NH_3 at 100 mbar (A), pyridine at vapor pressure (B), and 2,6-dTBP at vapor pressure (C) shown before (red curve) and after outgassing the probe molecules at room temperature (black curve).

The total number of accessible Brønsted acid sites (N) of HierSAPO-34 determined using the different probe molecules is reported in Table 4, along with the nature and position of the IR bands of their corresponding protonated species. From this data, it is evident that only a small fraction of the total Brønsted acid sites are accessible to the bulkier probe molecules but by introducing mesoporosity into CHA framework, the average micropore length is reduced and the number of accessible active sites increases accordingly. Unsurprisingly, pyridine is able to access a higher fraction of Brønsted acid sites than both 2,4,6-TMP and 2,6-dTBP, reflecting the smaller kinetic diameter of the former. The accessibility factor (AF) was also calculated for the pyridine derivatives. The AF is defined as the number of sites detected by adsorption of the alkylpyridine, divided by the total number of Brønsted acid sites detected by NH_3 adsorption. The AF value decreases with increasing alkylation of pyridine, correlating with increased steric bulk.

The catalytic activity of the HierSAPO-34 material was evaluated in the vapor-phase Beckmann rearrangement of cyclohexanone oxime to ε-caprolactam (the precursor to the Nylon-6 polymer) and contrasted with that of its microporous analogue. Under these conditions, the HierSAPO-34 shows exceptional catalytic performance, maintaining > 99 % conversion and ~ 95 % selectivity to the desired ε-caprolactam product over the course of the 6-hour reaction (Fig. 8A). The selectivity for ε-caprolactam is comparable between hierarchical and microporous SAPO-34 catalysts, which reflects the similarity in their acid characteristics and thus reinforces our spectroscopic evaluation (Fig. 8B). However, the overall activity of the HierSAPO-34 is vastly superior to its microporous analogue, even at short contact times. Notably, SAPO-34 achieves a maximum conversion of only ~ 82 %, which then steadily declines over course of the reaction, likely due to catalyst deactivation through pore-blockage [15].

This result suggests that, where the small pores of the CHA structure impede access to the internal acid active sites, catalysis is restricted to the more accessible Brønsted sites located on the exterior of the catalyst and at the pore mouths. As this reduces the number of active sites that available to participate in the catalytic reaction, maximal conversion is restricted.

Table 4. The concentration of accessible Brønsted acid sites (N) in HierSAPO-34

Probe molecules	Protonated species	Position of IR bands of protonated species	ε/ cm^2 $mmol^{-1}$	N/ mmol g^{-1}	AF
NH_3	NH_4^+	1450 (δ_{asym})	0.147 [53]	59.1	1
Pyridine	PyH^+	1545 (ν_{19b})	0.06 [54]	6.33	0.107
2,4,6-TMP	2,4,6-$TMPH^+$	1638 (ν_{8a})	0.62 [46]	2.24	0.038
2,6-dTBP	2,6-$dTBPH^+$	1618 (ν_{8a})	0.50 [47]	2.19	0.037

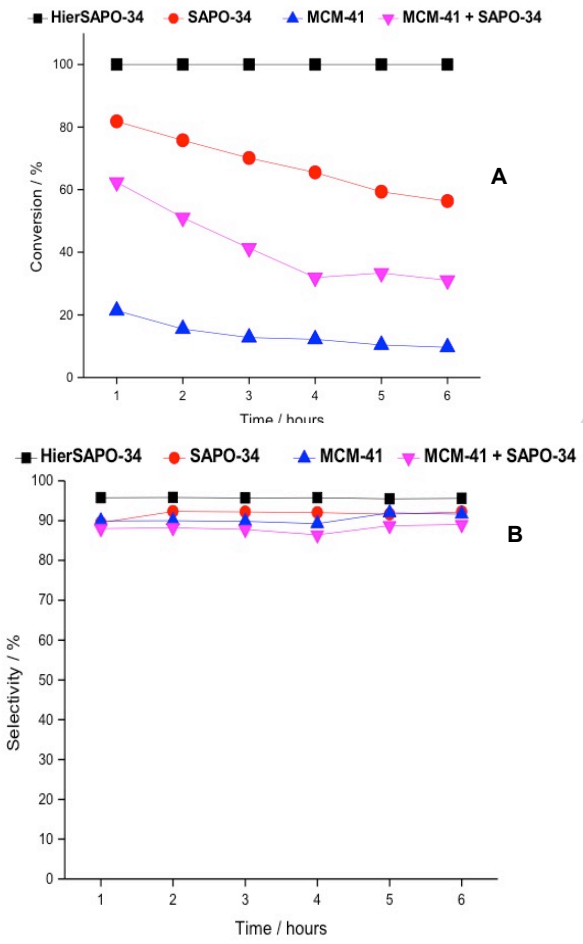

Figure 8. A comparison of the conversion of cyclohexanone oxime (A) and of selectivity towards ε-caprolactam oxime (B) in the vapor-phase Beckmann rearrangement, under acid catalysis, at 598 K and 0.79 h^{-1} WHSV.

To verify that the superior activity of HierSAPO-34 was not solely due to improved access to indiscriminate acid sites, mesoporous MCM-41 was also tested in the Beckmann rearrangement. MCM-41 contains pendant silanol groups that can participate in transformations that are catalyzed by weak acids. Thus, the consistently low conversion of cyclohexanone oxime, which successively declines over the course of the reaction, illustrates the importance of the nature of the Brønsted acid sites, as well as their accessibility, in facilitating the desired transformation in high yield. Moreover, the net conversion achieved by a 50:50 physical mixture of microporous SAPO-34 and MCM-41 appears as a summation of that of the individual frameworks, highlighting the importance of designing a single framework that amalgamates improved mass-transfer capabilities with desirable acid site properties.

Conclusions

CTAB encapsulated within MCM-41 has been used to template the design of hierarchical SAPO-34 without the need for sophisticated surfactant molecules. FTIR studies using CO as a molecular probe, in conjunction with solid-state MAS NMR studies, have revealed that the acid characteristics of microporous SAPO-34 are retained in our HierSAPO-34 material Moreover, FTIR studies of adsorbed alkylpyridines reveal the enhanced accessibility of the acid sites through the incorporation of an auxiliary mesoporous network. The findings from our catalytic study further demonstrate that our synthetic methodology effectively retains the desirable acid characteristics of the microporous analogue, whilst simultaneously enhancing mass transport capabilities through the introduction of secondary porosity. HierSAPO-34 shows superior catalytic activity in the acid-catalyzed vapor-phase Beckmann rearrangement of cyclohexanone oxime to ε-caprolactam, relative to both microporous SAPO-34 and to mesoporous MCM-41. Moreover, the mediocre yields of caprolactam achieved using a physical mixture of microporous SAPO-34 and mesoporous MCM-41 highlights the unique benefit in designing a single, homogenous hierarchical system that can host, contemporarily, both micro- and meso-pores. Our design strategy further vindicates a viable means of retaining the desirable acid characteristics of a parent microporous framework, whilst simultaneously improving the diffusion and mass-transport properties in catalytic transformations, offering wide-ranging benefits for diverse acid-catalyzed processes.

Experimental Section

Hierarchical SAPO-34 synthesis

Aluminium isopropoxide (7.00g, Sigma Aldrich) was added slowly to tetraethylammonium hydroxide (TEAOH) (14.00 ml, 35wt% in H_2O, Sigma Aldrich) under stirring. Deionized water (21 ml) was added and the mixture was stirred for 1 h. CTAB-containing MCM-41 (2.11 g, prepared as reported in ref. 23) was slowly added and the mixture was further stirred for 2 h. Phosphoric acid (2.33 ml, 85wt% in H_2O, Sigma Aldrich) was

added dropwise under stirring. The gel was vigorously stirred for 30 min to produce a white gel with the following composition:

1.0 Al: 1.0 P: 0.58 Si: 0.066 CTAB: 1 TEAOH: 50 H_2O

The gel was transferred to a Teflon-lined stainless-steel autoclave and crystallized at 473K for 60 h under autogenous pressure. The solid product from autoclave was then recovered by filtration and washed with water. The as-prepared product was dried in air at 373K and calcined in a tube furnace under air flow at 873K for 16h to remove organic surfactant and micropore template, producing a white crystalline solid.

Microporous SAPO-34 synthesis

Aluminium isopropoxide (7.00g, Sigma Aldrich) was added slowly to tetraethylammonium hydroxide (TEAOH) (14.00 ml, 35wt% in H_2O, Sigma Aldrich) under stirring. Deionized water (21 ml) was added and the mixture was stirred for 1 h. Tetraethylorthosilicate (TEOS) (1.14 ml, Sigma Aldrich) was added dropwise under stirring and the mixture was further stirred for 2 h. Phosphoric acid (2.33 ml, 85wt% in H_2O, Sigma Aldrich) was added dropwise under stirring. The gel was vigorously stirred for 30 min to produce a white gel with the following composition:

1.0 Al: 1.0 P: 0.15 Si: 1 TEAOH: 50 H_2O

The gel was transferred to a Teflon-lined stainless-steel autoclave and crystallized at 473K for 60 h under autogenous pressure. The solid product from autoclave was then recovered by filtration and washed with water. The as-prepared product was dried in air at 373K and calcined in a tube furnace under air flow at 873K for 16h to produce a white crystalline solid.

Characterization

Before undertaking structural, volumetric and spectroscopic analysis, calcined samples were outgassed at 573K to remove adsorbed water.

Scanning Electron Microscopy (SEM) images at different magnifications were recorded on a Quanta 200 FEI Philips Scanning Electron Microscope equipped with an EDAX energy dispersive spectroscopy (EDS) attachment. The electron source was a tungsten filament operating at 25 keV. The samples were coated with a thin gold layer to ensure surface conductivity.

X-ray powder diffraction (XRD) patterns were obtained using an ARL XTRA48 diffractometer with Cu Kα radiation (λ = 1.54062 Å).

For ICP-OES analyses, samples were digested under acidic conditions before being aspirated into the Varian Vista MPX CCD Simultaneous axial ICP-OES instrument.

N_2 physisorption measurements were carried out at 77 K in the relative pressure range from $1x10^{-6}$ to 1 P/P_0 by using a Quantachrome Autosorb1MP/TCD instrument. Prior to the analysis, the samples were outgassed at 573 K for 3 h (residual pressure lower than 10^{-6} Torr). Specific surface areas were determined using the BET equation, in the relative pressure range from 0.01 to 0.1 P/P_0. The desorption branch of the N_2 physisorption isotherm was analyzed by means of the NLDFT (non-local density functional theory) method, to obtain the pore size distribution of the materials.

Solid-state (SS) NMR spectra were acquired on a Bruker Avance III 500 spectrometer and a wide bore 11.7 Tesla magnet with operational frequencies for ^1H, ^{29}Si, ^{31}P and ^{27}Al of 500.13, 99.35, 202.45 and 130.33MHz, respectively. A 4mm triple resonance probe with magic angle spinning (MAS) was employed in all the experiments and the samples were packed on a Zirconia rotor and spun at a MAS rate of 15 kHz. The magnitude of radio frequency fields, μ_{rf}, were 100, 83 and 42 kHz for ^1H, ^{31}P and ^{29}Si, respectively. The ^{27}Al MAS spectra were acquired on large sweep width with small pulse angle ($\pi/12$) to ensure quantitative interpretation. In the case of ^{29}Si, ^{31}P and ^{27}Al MAS NMR, high-power proton decoupling was applied. The relaxation delay, d1, between accumulations was 5, 1, 20, and 60 s for ^1H, ^{27}Al, ^{31}P and ^{29}Si MAS NMR spectroscopy, respectively. All chemical shifts were reported by using δ scale and are externally referenced to TMS for ^1H and ^{29}Si NMR, $Al(H_2O)_6^{3+}$ ion in 1.0 m $AlCl_3$ solution for ^{27}Al NMR and H_3PO_4 (85%) for ^{31}P NMR. The chemical shifts reported for $^{27}A1$ are not corrected for second-order quadrupole effects.

^1H MAS NMR spectra were fitted with DMFIT functions for quantitative deconvolution of overlapping peaks. The samples were packed on a NMR rotor and dehydrated at 573K under vacuum ($1x\ 10^{-4}$ mbar) for 2 h prior to the loading into the magnet and recording of the NMR spectrum.

FTIR spectra of self-supporting pellets were collected under vacuum conditions (residual pressure $<10^{-5}$ mbar) using a Bruker Equinox 55 spectrometer equipped with a pyroelectric detector (DTGS type) with a resolution of 4 cm^{-1}. CO was adsorbed at 80 K and NH_3, 2,4,6-trimethylpyridine (2,4,6-TMP, collidine) and 2,6-di-*tert*-butylpyridine (2,6-dTBP) were adsorbed at room temperature using specially designed cells permanently connected to a vacuum line to perform adsorption–desorption *in situ* measurements. FTIR spectra were normalized with respect the pellet weight and, whenever specified, are reported in difference-mode by subtracting the spectrum of the sample in vacuum from the spectrum of the adsorbed molecules (CO and pyridine derivatives).

The total number of accessible Brønsted acid sites (N) was estimated using the Lambert–Beer law in the form $A = \varepsilon N \rho$, where A is the integrated area of the bands of the protonated species, ε is the molar extinction coefficient ($cm^2\ mmol^{-1}$), N is the concentration of the vibrating species (mmol g^{-1}), and ρ is the density of the disk (mass/area ratio of the pellet, mg cm^{-2}).

Catalysis

A cylindrical (4 mm diameter), quartz, fixed-bed reactor with a quartz frit was packed with 0.5 cm layer of glass beads (1mm). The catalyst (0.2 g) was pelletized and added to the reactor, followed by a further 20 cm of glass beads (1 mm). The reactor was transferred into the heater unit of the flow-reactor setup. The catalyst was pre-treated by heating at 673 K for 1 h under a 50 ml min^{-1} flow of helium gas. The temperature and flow of helium gas were then reduced to 598 K and 33.3 ml min^{-1}, respectively. A liquid-feed of 100 g L^{-1} of cyclohexanone oxime in ethanol was fed, *via* electronic syringe pump, into the reactor to maintain a weight hourly space velocity (WHSV) of 0.79 hr^{-1}. As an external standard, a liquid feed of 100 g L^{-1} of mesitylene

in ethanol was simultaneously introduced into the exit feed using WHSV of 0.79 hr^{-1}. Once steady-state was established, samples were collected on an hourly basis and analyzed using the Clarus 480 gas chromatograph with FID detector and Elite 5 column. Product formation was quantified against the mesitylene external standard.

Acknowledgements

This research is supported by the Compagnia di San Paolo (HEPYCHEM project). This project has received funding from the European Union's Horizon 2020 research and innovation programme under grant agreement N. 720783.The Engineering and Physical Sciences Research Council (EPSRC, UK) is gratefully acknowledged for resources and support provided via our membership of the UK Catalysis Hub Consortium (EP/K014706/1). SC also acknowledges Honeywell LLC for studentship funding. The authors thank C. Ivaldi for the support in the synthesis.

Keywords: Hierarchical SAPO-34, Brønsted acid sites, Beckmann rearrangement, physico-chemical characterization, adsorption of alkylpyridines.

References

[1] A. Corma, *Chem. Rev*. **1997**, *97*, 2373-2420.
[2] Z. Wang, Y. Yu, R. Xu, *Chem. Soc. Rev*. **2012**, *41*, 1729-1741.
[3] M. Hartmann, L. Kevan, *Chem Rev*. **1999**, *93*, 635-664.
[4] E. Gianotti, M. Manzoli, M.E. Potter, V.N. Shetti, D. Sun, J. Paterson, T.M. Mezza, A. Levy, R. Raja, *Chem. Sci*. **2014**, *5*, 1810-1819.
[5] M.A. Carreon, S. Li, J.L. Falconer, R.D. Noble, *J. Amer. Chem. Soc*. **2008**, *130*, 5412-5413.
[6] H. Hong, S. Li, J.L. Falconer, R.D. Noble, *J. Membr. Sci*. **2008**, *307*, 277-283.
[7] B. Vora, J.Q. Chen, A. Bozzano, B. Glover, P. Barger, *Catal. Today* **2009**, *141*, 77-83
[8] D. Chen, K. Moljordand, A. Holmen, *Micropor. Mesopor. Mater*. **2012**, *164*, 239-250.
[9] P. Tian, Y. Wei, M. Ye, Z. Liu, *ACS Catal*. **2015**, *5*, 1922-1938.
[10] X. Zhu, J.P. Hofmann, B. Mezari, N. Kosinov, L. Wu, Q. Qian, B.M. Weckhuysen, S. Asahina, J. Ruiz-Martinez, E.J.M. Hensen, *ACS Catal*. **2016**, *6*, 2163-2177.
[11] D. Verboekend, M. Milina, J. Perez-Ramirez, *Chem. Mater*. **2014**, *26*, 4552-4562.
[12] X. Chen, A. Vicente, Z. Qin, V. Ruaux, J-P. Gilson, V. Valtchev, *Chem. Commun*. **2016**, *52*, 3512-3515.
[13] D. Xi, Q. Sun, X. Chen, N. Wang, Y. Yu, *Chem. Commun*. **2015**, *51*, 11987-11989.
[14] C. Wang, M. Yang, P. Tian, S. Xu, Y. Yang, D. Wang, Y. Yuan, Z. Liu, *J. Mater. Chem. A* **2015**, *3*, 5608-5616.
[15] S.H. Newland, W. Sinkler, T. Mezza, S.R. Bare, M. Caravetta, I.M. Haies, A. Levy, S. Keenan, R Raja, *ACS Catal*. **2015**, *5 (11)*, 6587–6593.
[16] K. Na, M. Choi, R. Ryoo, *Micropor. Mesopor. Mater*. **2013**, *166*, 3–19.
[17] J.C. Groen, J.C. Jansen, A. Moulijn, J. Pérez-Ramìrez**,** *J. Phys. Chem. B* **2004,** *108,* 13062-13065.
[18] A. Erigoni, S.H. Newland, G. Paul, L. Marchese, R. Raja, E. Gianotti, *ChemCatChem* **2016**, *8*, 3161–3169.
[19] Q. Sun, N. Wang, D. Xi, M. Yang, J. Yu, *Chem. Commun.* **2014**, *50*, 6502-6505.
[20] D.P. Serrano, J.M. Escola, P. Pizarro, *Chem. Soc. Rev*. **2013**, *42*, 4004-4035.
[21] M.S. Holm, S. Svelle, F. Joensen, P. Beato, C.H. Christensen, S. Bordiga, M. Bjørgen, *Appl. Catal. A* **2009**, *356*, 23–30.
[22] K. Sadowska, K. Gorà-Marek, J. Datka, *J. Phys. Chem. C* **2013**, *117*, 9237–9244.
[23] D.R. Radu, C.-Y. Lai, K. Jeftinija, E.W. Rowe, S. Jeftinija, V.S.-Y. Lin, *J. Am. Chem. Soc.* **2004**, *126*, 13216–13217.
[24] E.A. Kang, T.-W. Kim, H.-J. Chae, M. Kim, K.-E. Jeong, J.-W Kim, C.-U. Kim, S.-Y. Jeong, J. *Nanosci. Nanotechnol*. **2013**, *13*, 7498-7503.
[25] J. Landers, G.Y. Gor, A.V. Neimark, *Colloids Surf. A: Physicochem. Eng. Aspects* **2013**, *437*, 3-32.
[26] M. Thommes, K.A. Cychosz, *Adsorption* **2014**, *20*, 233-250
[27] M. Errahali, G. Gatti, L. Tei, G. Paul, G.A. Rolla, L. Canti, A. Fraccarollo, M. Cossi, A. Comotti, P. Sozzani, L. Marchese, *J. Phys. Chem. C* **2014**, *118*, 28699-28710.
[28] B. Zibrowius, E. Loffler, M. Hunger, *Zeolites* **1992**, *12*, 167-174.
[29] W. Lutz, R. Kurzhals, S. Sauerbeck, H. Toufar, J.-C. Buhl, T. Gesing, W. Altenburg, C. Jäger, *Micropor. Mesopor. Mater*. **2010**, *132*, 31–36.
[30] a) G.A.V.Martins, G. Berlier, S. Coluccia, H.O. Pastore, G.B. Superti, G. Gatti, L. Marchese, *J. Phys. Chem. C* **2007,** *111,* 330-339. b) G.A.V. Martins, G. Berlier, C. Bisio, S. Coluccia, H.O. Pastore, L. Marchese, *J. Phys. Chem C* **2008**, *112*, 7193-7200.
[31] A. Buchholz, W. Wang, A. Arnold, M. Xu, M. Hunger, *Micropor. Mesopor. Mater*. **2003**, *57*, 157-168.
[32] L. Smith, A.K. Cheetham, L. Marchese, J.M. Thomas, P.A. Wright, J. Chen, E. Gianotti, *Catal. Lett*. **1996**, *41*, 13−16.
[33] S. Bordiga, L. Regli, C. Lamberti, A. Zecchina, M. Jorgen, K.P. Lillerud, *J. Phys. Chem. B* **2005**, *109*, 7724−7732.
[34] M. Hunger, S. Ernst, S. Steuernagel, J. Weitkamp, *Micropor. Mater*. **1996**, *6*, 349-353.
[35] M. Hunger, J. Kärger, H. Pfeifer, J. Caro, B. Zibrowius, M. Bülow, R. Mostowicz, *J. Chem. Soc., Faraday Trans.* **1987**, *83*, 3459-3468.
[36] M. Hunger, M.W. Anderson, A. Ojo, H. Pfeifer, *Micropor. Mater*. **1993**, *1*, 17-32.
[37] J. Trébosc, J.W. Wiench, S. Huh, V.S.-Y. Lin, M. Pruski, J. *Am. Chem. Soc*. **2005**, *127*, 3057-3068.
[38] M.A. Makarova, A.F. Ojo, K. Karim, M. Hunger, J.J. Dwyer, *J. Phys. Chem* **1994**, *98*, 3619–3623.
[39] H. Knözinger, S.J. Huber, *J. Chem. Soc. Faraday Trans*. **1998**, *94*, 2047–2059.
[40] K. Chakarova, K. Hadjiivanov, *J. Phys. Chem. C* **2011**, *115*, 4806–4817.
[41] M.E. Potter, M.E. Cholerton, J. Kezina, R. Bounds, M. Carravetta, M. Manzoli, E. Gianotti, M. Lefenfeld, R. Raja, *ACS Catalysis* **2014**, *4*, 4161-4169.
[42] E. Gianotti, V. Dellarocca, E.C. Oliveira, S. Coluccia, H.O. Pastore, L. Marchese, *Stud. Surf. Sci. Catal*. **2002**, *142*, 1419−1426.
[43] Y. Izumi, H. Ichihashi, Y. Shimazu, M. Kitamura, H. Sato, *Bull. Chem. Soc Jpn*. **2007**, *80*, 1280–1287
[44] F. Thibault-Starzyk, I. Stan, S. Abellò, A. Bonilla, K. Thomas, C. Fernandez, J-P. Gilson, J. Perez-Ramirez, *J. Catal.* **2009**, *264*, 11–14.
[45] F. Thibault-Starzyk, A. Vimont, J.-P. Gilson, *Catal. Today* **2001**, *70*, 227–241.
[46] K. Mlekodaj, K. Tarach, J. Datka, K. Gòra-Marek, W. Makowski, *Micropor Mesopor. Mater.* **2014**, *183*, 54–61 .
[47] K. Gòra-Merek, K. Tarach, M. Choi, *J. Phys. Chem. C* **2014**, *118*, 12266-12274.
[48] J.F. Arenas, I. Lòpez Tocòn, J.C. Otero, J.I. Marcos, *J. Mol. Struct*. **1999**, *476*, 139-150.
[49] C. Morterra, G. Cerrato,. G. Meligrana, *Langmuir* **2001**, *17*, 7053–7060.
[50] J.M.R. Gallo, C. Bisio, G. Gatti, L. Marchese, H.O. Pastore, *Langmuir* **2010**, *26(8)*, 5791–5800.

[51] A. Zecchina, L. Marchese, S. Bordiga, C. Pazè, E. Gianotti, *J. Phys. Chem B* **1997,** *101*, 10128-10135.
[52] R. Buzzoni, S. Bordiga, G. Ricchiardi, C. Lamberti, A. Zecchina, *Langmuir* **1996**, *12*, 930-940.
[53] J. Datka, B. Gil, A. Kubacka, *Zeolites* **1995**, *15*, 501-506.
[54] J. Datka, *J. Chem. Soc., Faraday I* **1980**, *76*, 2437-2447.

10.1002/chem.201701978

WILEY-VCH

Entry for the Table of Contents (Please choose one layout)

Layout 1:

FULL PAPER

Hierarchical SAPO-34 has been synthesized with a distinctive bottom-up approach using CTAB encapsulated within ordered mesoporous silica that serves as both the silicon source and mesoporogen

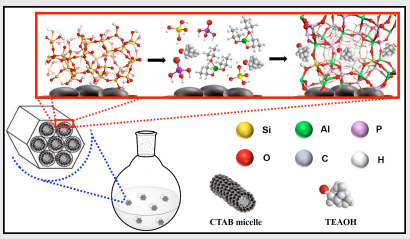

*I. Miletto,[1] G. Paul, S. Chapman, G. Gatti, L. Marchese, R. Raja and E. Gianotti**

Page No. – Page No.

Mesoporous silica scaffolds as precursor to drive the formation of hierarchical architectures with tunable acid properties

Layout 2:

FULL PAPER

((Insert TOC Graphic here; max. width: 11.5 cm; max. height: 2.5 cm))

*Author(s), Corresponding Author(s)**

Page No. – Page No.

Title

Text for Table of Contents